JACS
JOURNAL OF THE AMERICAN CHEMICAL SOCIETY
Article
pubs.acs.org/JACS

Dynamic Anchoring of the 3′-End of the Guide Strand Controls the Target Dissociation of Argonaute–Guide Complex

Seung-Ryoung Jung,[†,‡,⊥] Eunji Kim,[∥,⊥] Wonseok Hwang,[†,‡] Soochul Shin,[§] Ji-Joon Song,*[,∥] and Sungchul Hohng*[,†,‡,§]

[†]Department of Physics and Astronomy, [‡]National Center for Creative Research Initiatives, and [§]Department of Biophysics and Chemical Biology, Seoul National University, Seoul 151-747, Korea

[∥]Department of Biological Sciences, KAIST, Daejeon 305-701 Korea

Supporting Information

ABSTRACT: Argonaute (Ago) is the catalytic core of small RNA-based gene regulation. Despite plenty of mechanistic studies on Ago, the dynamical aspects and the mechanistic determinants of target mRNA binding and dissociation of Ago–guide strand remain unclear. Here, by using single-molecule fluorescence resonance energy transfer (FRET) assays and *Thermus thermophilus* Ago (*Tt*Ago), we reveal that the 3′-end of the guide strand dynamically anchors at and releases from the PAZ domain of Ago, and that the 3′-end anchoring of the guide strand greatly accelerates the target dissociation by destabilizing the guide–target duplex. Our results indicate that the target binding/dissociation of Ago–guide is executed through the dynamic interplays among Ago, guide, and target.

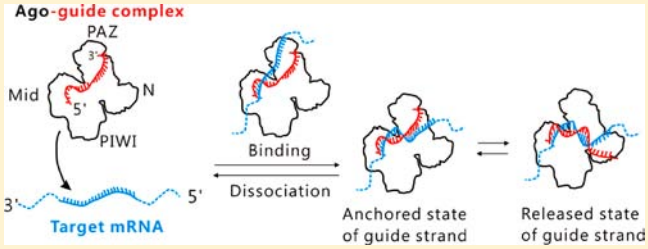

INTRODUCTION

Small RNAs including small interfering RNAs (siRNAs), microRNAs (miRNAs), and piwi-interacting RNAs (piRNAs) play crucial roles in gene regulation.[1−5] Though their biogenesis pathways and biological functions are distinct,[6] small RNAs are incorporated into the same Ago protein family to form an effector complex such as RNA-induced silencing complex (RISC),[7] and RNA-induced transcriptional silencing complex (RITS), rendering Ago a core enzyme for all small RNA-related gene silencing pathways.

RISC is loaded with a double-stranded miRNA or siRNA, and then maturated by ejecting one strand (the passenger strand) while maintaining the other strand (the guide strand).[8] The RISC maturation occurs in two distinct pathways. In the slicer-dependent pathway, the dissociation of the passenger strand is facilitated by cleavage of the passenger strand by Ago. The mechanism of the slicer-independent pathway is not fully understood yet, but it is evident that Ago plays an essential role in this pathway.[9,10] Mature RISC recognizes its target messenger RNA (mRNA) based on the guide–target sequence complementarity and the accessibility of the target site.[1,2,11−15] RISC-mediated translational regulation occurs again via either a slicer-dependent pathway or a slicer-independent pathway.[16] In either pathway, efficient unwinding of guide–mRNA duplexes is crucial for the multiple-turnover catalytic activity of RISC in the slicer-dependent pathway[17] and for efficient off-target release in the slicer-independent pathway. Therefore, interconversion of RISC between a double-stranded RNA-bound form and a single-stranded RNA-bound form is a fundamental process for both RISC maturation and translational regulation by RISC.

To understand how the two opposite activities of Ago (i.e., unwinding and annealing of RNAs) are coordinated in RISC, extensive studies employing diverse approaches have been performed. Especially, structural studies on prokaryotic Ago proteins have been pivotal to our understanding of how RISC recognizes its target.[18−22] The first crystal structure of a full-length Ago revealed that the protein is composed of four domains: N-terminal, PAZ, MID, and PIWI domains.[19] On the basis of the fact that the PIWI domain had an RNaseH fold, it was suggested that the PIWI domain was responsible for the slicer activity of RISC,[19] which was confirmed by later biochemical and mutagenesis studies.[23,24] Various crystal structures revealed that both the 3′-end and the 5′-end of the guide strand are anchored at the PAZ domain and in the MID-PIWI interface, respectively.[18,20,21,25−27] This observation provided a natural explanation for why a 5′-end phosphate group and a 3′-end dinucleotide overhang are required for RISC loading of miRNAs and siRNAs.[28−30] Furthermore, the Ago–guide binary complex structure showed that g2–g6 nucleotides (in this work we refer the nucleotides of guide (g) and target (t) strands from the 5′-to-3′ perspective of the guide strand. Therefore, g2 and t2 refer to the second nucleotide from the 5′-end of the guide strand and its base pairing nucleotide of the target strand, respectively) are preorganized in A-form and exposed to the solvent side for

Received: April 8, 2013
Published: October 14, 2013

 © 2013 American Chemical Society dx.doi.org/10.1021/ja403138d | J. Am. Chem. Soc. 2013, 135, 16865−16871

ready base-pairing with a target RNA.[21] This observation was consistent with the previous biochemical and bioinformatic studies indicating that target specificity is mainly determined by a sequence complementarity in the seed region of the guide strand (g2-g8),[11,12,15] and the biophysical study showing that preorganization of the seed region of the guide strand in RISC makes the target recognition process favorable by reducing the entropic cost of the guide−target base pairing.[31]

On the basis of these observations, it was suggested that the guide−target base pairing nucleates in the seed region, and then propagates to the 3′-end of the guide strand. However, the structure of Ago−guide binary complexes, in which the 3′-end of the guide strand is anchored at the PAZ domain, was not compatible with a completely base-paired oligonucleotide duplex in A-form, suggesting that extensive conformational changes of the Ago−guide complex would occur during the base pair propagation. Regarding the structural rearrangement of RISC during the base pair propagation, different models have been considered. In the 'fixed-end' model, Ago experiences a structural change while the 3′-end of the guide strand remains anchored to the PAZ domain.[32,33] On the other hand, the 'two-state' model predicts that the 3′-end of the guide strand is released from the PAZ domain to allow full base pairing of the guide and target strands;[32,33] the two-state model does not necessary requires the movement of the PAZ domain after the target binding while the fixed-end model would require substantial movement of the PAZ domain. The two-state model was supported by a recent structural study showing that the 3′-end of the guide strand was released when base pairing was established up to 16th bases.[34] Interestingly, based on the fact that Ago has dual functions of RNA unwinding for RISC maturation and annealing for target recognition, it was recently proposed that the 3′-end of the guide strand is in dynamic equilibrium between the anchored state and the released state.[8] Compared to the originally proposed static two-state model, we term this model the dynamic two-state model.

Despite these remarkable advances in our understanding of how Ago interacts with its guide and target strands, the insightful crystal structures of Ago−oligonucleotide complexes may represent only a particular conformation of a dynamic conformational ensemble. In the absence of a direct characterization of RNA annealing/unwinding kinetics and intrinsic conformational dynamics of RISC, it is still unclear how the RNA annealing and RNA unwinding activities of Ago are regulated by structural features such as guide−target mismatches and terminal anchoring of the guide strand. Here we used single-molecule fluorescence resonance energy transfer (FRET) assays[35] to address the questions above. On the basis of the following considerations, a minimal complex composed of *Thermus thermophilus* Ago (*Tt*Ago) and a guide DNA was selected as a model system. First, *Tt*Ago already has rich structural and biochemical information that can be readily compared to the results of our single-molecule experiments.[21,22,24] Second, the presence of just two natural cysteines in *Tt*Ago facilitated the dye-labeling of the protein by mutagenesis with negligible side effects. Furthermore, recent structures of eukaryotic Ago proteins[36−38] show that most of the structural features observed in *Tt*Ago−oligonucleotide complexes are evolutionarily conserved in higher organisms.

RESULTS

Single-Molecule FRET Assay To Monitor the Interaction of Ago−Guide and Its Target. To study target binding and dissociation dynamics of Ago−guide complex by using single-molecule FRET, we designed oligonucleotide sequences based on let-7 miRNA (Figure 1a). The guide

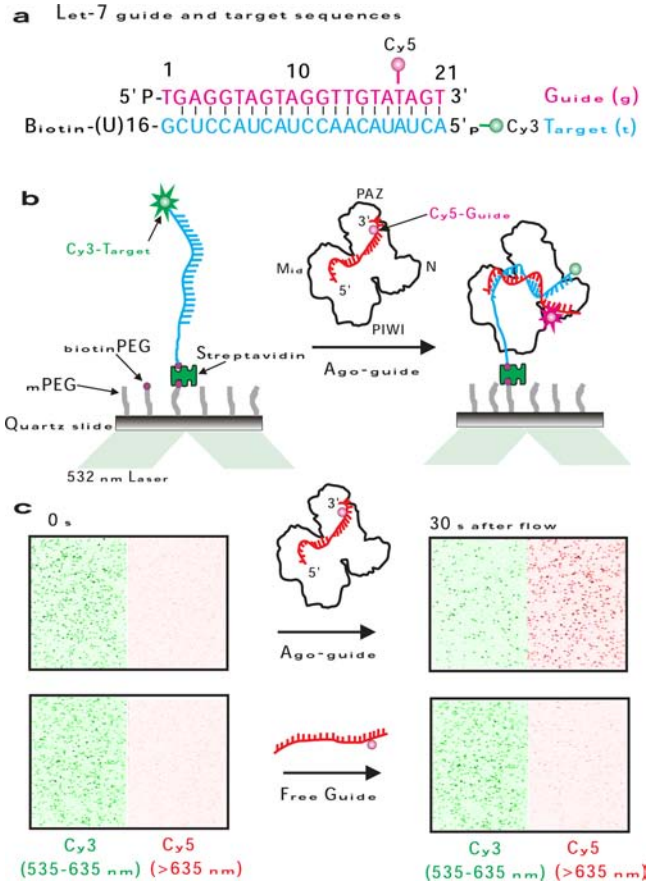

Figure 1. Single-molecule FRET experiments for the observation of Ago−guide−target interaction. (a) Oligonucleotide design. Guide DNA sequence (top) was borrowed from let-7 miRNA. Target RNA sequences with varying mismatches were used, but only the target RNA sequence with full complementarity (no mismatch target except 1st base pairing) is shown (below). The information of sequences is available in Materials and Methods. (b) Experimental scheme. After immobilizing Cy3-labeled target RNA, we added preassembled Cy5-labeled guide−Ago complexes and monitored individual binding events of Ago−guide to the target via single-molecule FRET. (c) Single molecule images of donor channel (green, 535−635 nm) and acceptor channel (red, > 635 nm) before (left) and 30 s after Ago−guide (2 nM) injection (right). The molecules were excited at 532 nm. The case when free guide strand (2 nM) was added is compared below. (T = 45 °C, [$MgCl_2$] = 1 mM, [KCl] = 135 mM).

DNA was labeled with a FRET acceptor (Cy5) at the 18th base (Materials and Methods). The target RNA was labeled with a FRET donor (Cy3) at the 5′-end phosphate and a biotin at the 3′-end (Materials and Methods). The target strand has a spacer (a 16-nt uridine stretch) between the biotin and the target sequence to avoid any steric hindrance due to surface immobilization. We were able to measure the slicer activity of *Tt*Ago with these modified strands (Figure S1) and confirmed that the modifications do not significantly hinder the kinetics of the slicer activity of *Tt*Ago (Figure S2).

For single-molecule FRET experiments, the Cy3-labeled target strand was immobilized on a polymer-coated quartz surface via biotin-streptavidin interaction, and then preas-

dx.doi.org/10.1021/ja403138d | J. Am. Chem. Soc. 2013, 135, 16865−16871

sembled Ago–guide complexes were added into the detection chamber (Figure 1b). Changes in fluorescence intensities were monitored over time in a total-internal-reflection fluorescence microscope. Upon successful target recognition of Ago–guide, Cy3 signal is expected to drop simultaneously with Cy5 signal jump due to FRET. After adding 2 nM Ago–guide (we assumed all guide strands were complexed with Ago, Figure S3), we observed fast appearance of Cy5 spots and simultaneous disappearance of Cy3 spots (Figure 1c, top). In contrast, when the guide strand alone (2 nM) was added, the guide–target binding rate was much slower than that of Ago–guide complex (Figure 1c, bottom), indicating that target recognition is greatly accelerated when a guide strand is incorporated in Ago.

Kinetics of Ago–Guide and Target Interaction. To quantitatively understand how Ago affects the dynamics of the guide–target interactions, we compared binding and dissociation kinetics of Ago–guide or free-guide. It was obvious that the guide–target interaction was dynamic when the guide strand was complexed with *Tt*Ago (Figure 2a and Figure S4).

The kinetics analysis revealed that the binding rate of Ago–guide increased 21-fold compared with that of free-guide (Figure 2b). The dissociation time of Ago–guide (Figure 2c) cannot be compared with that of free guide because the free guide–target duplex was too stable to be directly measured in real time. The histograms of binding and dissociation time were well fitted to single exponential functions (Figure 2b,c). In addition, stable long binding events of free guide (Figure 2a, bottom) were hardly observed in the Ago–guide experiments. Therefore, we concluded that contamination of free guide was negligible in the Ago–guide experiment. As expected from binding/dissociation events of single Ago–guide complex, the binding rate was linearly increased with Ago–guide concentration, while the dissociation rate was more or less the same in the examined concentration range (Figure 2d and Figure S5).The *y*-intercept of the binding rate was close to zero, indicating that photobleaching affects little to our analysis. Of note, we also tested binding events of *TtAgo* loaded with guide RNA. Because of low affinity of guide RNA to *TtAgo*, significant contamination of free guide binding was observed (Figure S6). Interestingly, however, we observed that binding rate was accelerated by 5-fold in the presence of *TtAgo* compared to the free RNA guide, indicating *TtAgo* can efficiently help the target search of the RNA guide strand once it is loaded on *TtAgo* (Figure S6).

The observations in Figure 2 reveal that *Tt*Ago accelerates not only target binding but also target dissociation. Interestingly, recent crystal structure of *Tt*Ago–guide–target ternary complex showed that full base pairing of guide and target strands was blocked by the presence of N-terminal domain of *Tt*Ago.[34] Consistent with the report, FRET efficiency between guide and target strands in the Ago–guide–target ternary complex (E = 0.81 vs 0.97) was smaller than that in the free guide–target duplex (Figure 2a, right). Indicating that the 3′-end region of the guide strand is not very important for target recognition, mismatches introduced to the 3′-end of the guide strand only mildly affected the binding and dissociation rates (Figure S7). Recently, it has been reported that the guide–target duplex is destabilized by fly and mouse Agos,[39] indicating that prokaryotic and eukaryotic Agos share common features. Additionally, we note that the target dissociation of Ago–guide reported in this article should be considered as slicer-independent since all experiments were performed at temperatures (23 or 45 °C, denoted in figure legends) where the slicer activity of *Tt*Ago is inhibited (Figure S1).

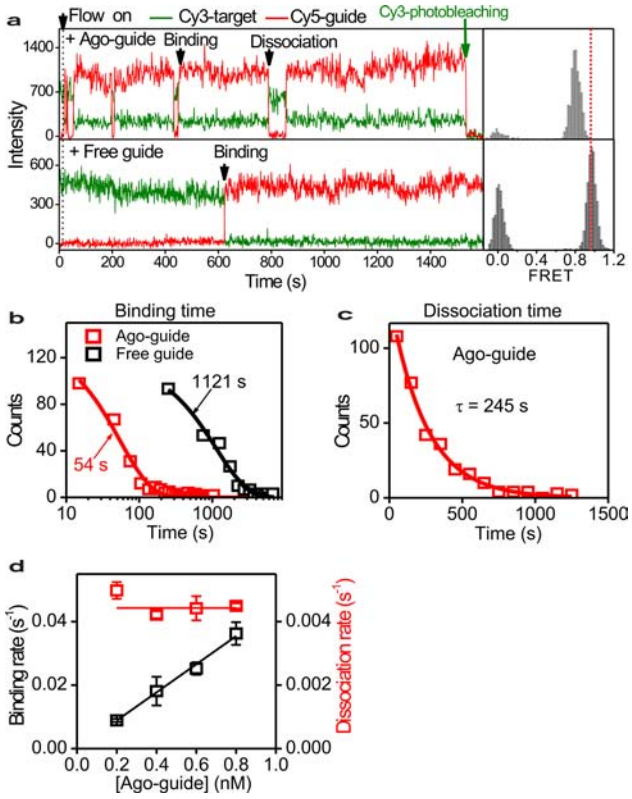

Figure 2. Acceleration of target binding/dissociation kinetics by Ago. (a) Representative fluorescence intensity time traces of Cy3 (green) and Cy5 (red) when Ago–guide (0.4 nM) was added at a time point denoted by an arrowhead (left), and corresponding FRET histogram (right). The case when free–guide (0.4 nM) was added is compared below. The experiments were preformed under the condition that the photobleaching time (4800 s; for 3600 s, 47% of molecules survived photobleaching) was much larger than the target dissociation time of Ago–guide. (b) Binding time histograms of Ago–guide (red) and free guide (black) obtained from the above experiments. Black and red lines indicate the single exponential fits of the data. (c) Dissociation time histogram of Ago–guide. (d) Ago–guide concentration dependence of the binding and dissociation rates. For the analyses in (c) and (d), dwell times were collected between binding events. The rates were obtained by inversing the time constants of the fitting graphs in Figure S5. (T = 45 °C, [$MgCl_2$] = 1 mM, [KCl] = 135 mM).

Dynamic Anchoring of the 3′-End of the Guide Strand. As alluded to earlier, the fate of the 3′-end of the guide strand in Ago after target recognition—whether it remains bound to the PAZ domain or not—has not been clearly delineated yet.[32,33] To address the question via single-molecule FRET, we prepared *Tt*Ago labeled with Alexa750 at the PAZ domain (see Materials and Methods). The dye-labeled *Tt*Ago exhibited a similar slicer activity kinetics as the wild type *Tt*Ago (Figure S2), indicating that the modifications (the replacement of the two natural cysteines with serines and the introduction of a new cysteine and its subsequent labeling) did not cause a significant hindrance to the enzymatic activity of *Tt*Ago. If the guide strand remains bound to the PAZ domain after target binding as predicted in the fixed-end model, high FRET is expected between Cy5 on the guide strand and Alexa750 labeled at the PAZ domain (Figure 3a). In case the

dx.doi.org/10.1021/ja403138d | J. Am. Chem. Soc. 2013, 135, 16865–16871

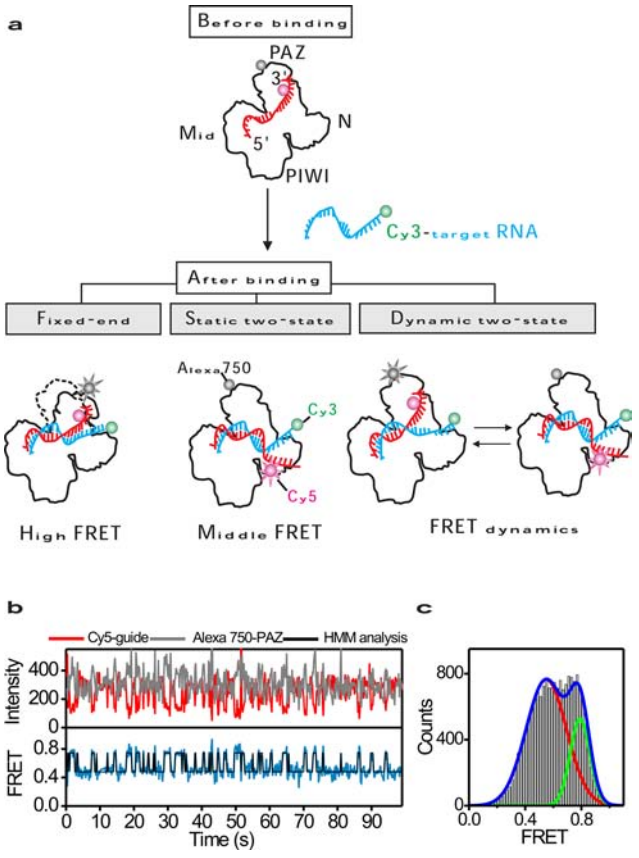

Figure 3. Repetitive anchoring of the 3′-end of the guide strand within the PAZ domain of Ago. (a) Scheme to distinguish the fixed-end model, the static two-state model, and the dynamic two-state model. Ago labeled with Alexa750 at the PAZ domain was used. (b) Representative fluorescence intensity time traces (top) of Cy5 (red) and Alexa750 (gray) and corresponding FRET time trace (blue, bottom). The FRET time trace was overlaid with a time traces generated by a two-state Hidden Markov modeling (black, bottom, HMM analysis). (c) FRET histogram of PAZ–guide dynamics collected from all triply labeled complexes (58 molecules). The solid lines are two-Gaussian fit of the data. (T = 23 °C for (a) and (b), [$MgCl_2$] = 1 mM, [KCl] = 135 mM).

3′-end of the guide strand is released after target binding as predicted in the static two-state model (Figure 3a), decreased Cy5–Alexa750 FRET is expected. On the other hand, the dynamic two-state model predicts FRET dynamics of the Cy5–Alexa750 FRET pair (Figure 3a). To determine which model is valid, we performed single-molecule three-color FRET experiments.[40] The triply labeled Ago–guide–target complex was formed in a detection chamber, and Cy3 and Cy5 were alternatively excited by using a green laser and a red laser, respectively. The existence of Cy3 was used to exclude nonspecifically bound Ago–guide complexes from data analysis, and FRET between Cy5 and Alexa750 was used to monitor the PAZ–guide dynamics in the ternary complex. Consistently with the dynamic two-state model, we observed fast dynamics of Cy5–Alexa750 FRET (Figure 3b). Such FRET dynamics were observed from most molecules analyzed: from 113 ternary complexes, 90 molecules (79.6%) showed two-state FRET dynamics while 20 molecules (17.7%) and 3 molecules (2.7%) showed stable middle FRET and stable high FRET, respectively. It seems that more than two released states—major middle FRET state (FRET efficiency E = 0.6) and minor low FRET state (E = 0.4)—exist in dynamic molecules (Figure S8). To understand what they represent, more studies are required. All data in this work were analyzed by assuming there are two states (i.e., the anchored and the released). A FRET histogram generated from all molecules, either dynamic or static, was nicely fitted to a sum of two Gaussian functions (Figure 3c), indicating an existence of two dominant conformational species. We observed the slicing kinetics was accelerated by dye-labeling of guide and target strands (Figure S2). Since it is believed that the slicing reaction occurs in the released state, we speculate that dye labeling increased the slicing activity of *Tt*Ago by enhancing the release of the guide strand. However, the increment was just 2-fold. Assuming that the released state population was affected by the same amount (in this case, from 38% to 76%), it is not probable that the releasing-anchoring dynamics of the guide strand appeared solely due to dye-labeling. We also found that the anchored state population was only mildly affected by the 3′-end mismatches (Figure S7).

We wondered why FRET dynamics observed between the PAZ domain and the guide strand was not observed between guide and target strands (Figure 2a). Currently, it is not known where the 3′-end of the guide strand is positioned in the released state. Speculating that the distance between the 3′-end of guide strand and the 5′-end of the target strand does not change very much after the release of the guide strand in the original sample design, we performed single-molecule FRET experiments with different guide length and dye-labeling positions, and could observe FRET dynamics between guide and target strands (Figure S9), reconfirming the dynamic two-state model.

Correlation between the 3′-End Anchoring and the Target Release. The observations in Figure 3 are a first direct demonstration of the dynamic two-state model during Ago–guide–target interaction. Then, what can be a biological function of these dynamics? In the original proposal of the dynamic two-state model, it was suggested that the passenger strand is more favorably ejected in the anchored state.[8] We investigated whether the target dissociation is correlated with the anchoring of the 3′-end of the guide strand; the anchoring/releasing dynamics of the guide strand could be monitored via FRET while the binding/dissociation of Ago–guide complex from the target was monitored via appearance/disappearance of fluorescence signals.

To observe target dissociation events of Ago–guide more frequently, we used mis:10–11 as a target for this experiment (Figure 4a, top). Representative fluorescence intensity and corresponding FRET time traces (Figure 4a and Figure S10) show that target dissociation mainly occurred in the anchored state. As a FRET efficiency histogram collected at the point of target dissociation shows (Figure 4b), such a correlation was generally observed in most molecules analyzed. A similar correlation was also observed from the fully complementary target RNA as well (Figure S11). Target dissociation was not observed from small number of Ago–guide complex which did not show FRET dynamics, and we suspect that these static molecules might be inactive. In addition, we observed that target binding occurs when the 3′-end of the guide strand is anchored to the PAZ domain (Figure S12), and concluded that the release of the 3′-end of the guide strand is initiated only after the target binding of Ago–guide. On the basis of our data, we postulated that the dissociation of Ago–guide from a target would be negatively affected when the 3′-end anchoring of the

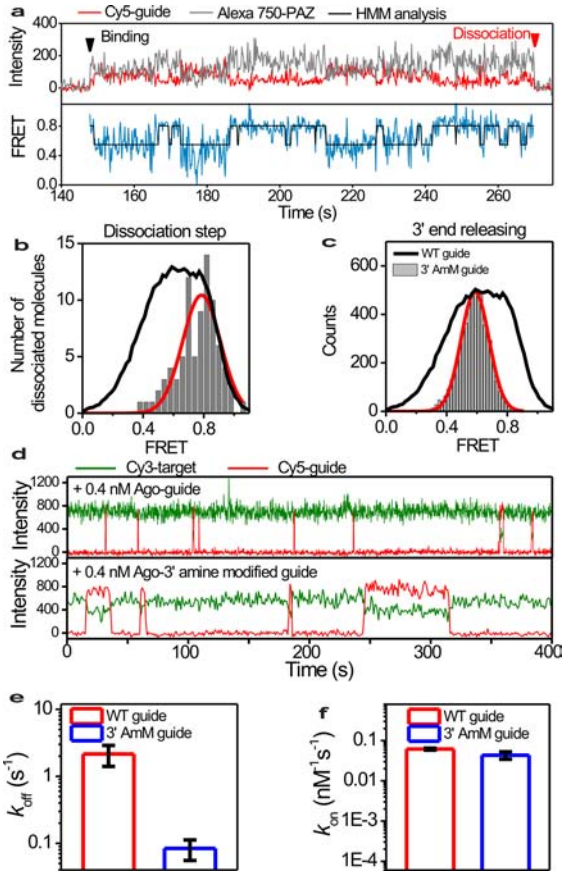

Figure 4. Correlation between the 3′-end anchoring of the guide strand and target (mis:10−11) dissociation. (a) Representative fluorescence intensity (top) and corresponding FRET time traces (blue, bottom) showing target binding/dissociation and anchoring/releasing of the 3′-end of the guide strand. The FRET time trace was overlaid with a time trace generated by a two-state Hidden Markov modeling (black, bottom, HMM analysis). The binding and dissociation of molecule are denoted by black and red arrow heads, respectively. (b) FRET efficiency histogram of Cy5−Alexa750 pair at the point of target release (gray bars, 84 molecules). The red lines are a Gaussian fit of the data denoted by gray bars. Black lines are Cy5−Alexa750 FRET histogram collected from whole duration of target binding of all triply labeled complexes (237 molecules). Interestingly, it is noticeable that the existence of the low FRET state (E = 0.4) is clearer with mis:10−11 than with the no mismatch target. (c) Cy5−Alexa750 FRET histogram for the guide whose 3′-end was modified by amine (3′AmM guide, gray bars). When compared to the case of the guide strand without the amine modification (WT guide, black lines), the anchored state population (interestingly the heterogeneity of the released state as well) was significantly decreased. (d) Representative fluorescence intensity time traces showing the extended dissociation time of the 3′-end amine-modified guide complexed with Ago ([Ago−guide] = 0.4 nM). (e) Effect of the 3′-end amine modification on the dissociation rate constant (k_{off}). (f) Effect of the 3′-end amine modification on the binding rate constants (k_{on}). The binding rate constants were obtained by dividing the binding rates with the concentration of Ago−guide. (T = 23 °C for (a−c) and 45 °C for (d−f), [$MgCl_2$] = 1 mM, [KCl] = 135 mM).

guide strand is hindered. To test the hypothesis, we hindered the 3′-end anchoring of the guide strand by introducing an amine group[41] with six carbon linker to the 3′ OH at g21 (the 3′ OH of g21 interacts with H227 and P255 in the PAZ domain of *Tt*Ago,[21] Figure S13) and examined FRET between the guide strand and the PAZ domain as well as the dissociation of Ago−guide from the target. As expected, the anchoring/releasing equilibrium was obviously biased to the released state by the introduction of the amine modification (Figure 4c), and target dissociation was significantly impaired (Figure 4d, 4e, and Figure S14). The amine modification of the guide strand did not affect the target binding rate of Ago−guide (Figure 4f and Figure S14), indicating that the 3′-end anchoring of the guide strand is not a prerequisite for the target binding of Ago−guide.

■ DISCUSSION

The early structural and biochemical studies showed that the PAZ domain recognizes the 3′-end of the guide strand, but it has not been clear what functional roles of the interaction between the PAZ domain and the 3′-end of the guide strand have. Our single-molecule FRET experiments showed that the interaction between the PAZ domain and the guide is not static but highly dynamic while Ago−guide is bound to the target, and more importantly that the target dissociation is strongly coupled to the 3′-end anchoring of the guide strand to the PAZ domain. Therefore, we infer that the PAZ domain plays critical roles for RISC maturation and target recognition by facilitating the dissociation of the passenger strand and off-targets, respectively. Our observation provides a reasonable explanation for the recent study that the PAZ domain is required for slicer-independent function of Ago.[42]

■ CONCLUSION

By using a single-molecule fluorescence assay and *Tt*Ago, we characterized the internal conformational dynamics of Ago−guide, and explained how a target strand is ejected in the slicer-independent pathway. Since many functional and structural features observed in prokaryotic Ago proteins are evolutionarily conserved in eukaryotic Ago proteins,[36−38] we expect that their core mechanisms will be similar. Thermophile proteins crystallized at low temperature have successfully provided structural insights of their operational mechanisms at their physiologically relevant temperature. Therefore, we further believe that *Tt*Ago will behave similarly at higher temperature (75 °C) except the differences in kinetic parameters of the reactions.

■ MATERIALS AND METHODS

Protein Preparation and Dye Labeling. *T. thermophilus* Ago (*Tt*Ago) gene was cloned into a modified pET28a vector generating an N-terminal His-tagged form. Ago was expressed in *Escherichia coli* BL21(DE3) cells with 0.5 mM IPTG at 18 °C. The cells expressing *Tt*Ago protein were lysed by sonication in a lysis buffer containing 1 M NaCl, 20 mM Tris-HCl (pH 7.5) and 2 mM $MgCl_2$. The lysed cells were centrifuged at 18 000 rpm for 1 h and the supernatant was incubated with Ni-NTA agarose resin (Qiagen) at 4 °C for 3 h. The Ni-NTA resin was then washed with the lysis buffer with 20 mM imidazole. *Tt*Ago protein was eluted with a buffer containing 500 mM NaCl, 20 mM Tris-HCl (pH 7.5), 2 mM $MgCl_2$ and 100 mM imidazole, and the N-terminal His-tag was removed by TEV protease treatment. Thermostable *Tt*Ago protein was further purified with heat-treatment at 55 °C for 15 min. After heat-treatment, *Tt*Ago protein in soluble fraction were collected and further purified with Superdex 200 (GE Healthcare) size exclusion column. To label the PAZ domain of Ago, we mutated all two natural cysteine residues to serines (C175S and C492S). In addition, one cysteine was introduced by mutating glycine 220 (G220C) to cysteine in the PAZ domain for labeling with maleimide-Alexa750 dye. All mutant proteins were purified as the wild type protein described above. For dye labeling of the PAZ domain of Ago, it was done by adding maleimide-Alexa750 (100 μM) to the

dx.doi.org/10.1021/ja403138d | J. Am. Chem. Soc. 2013, 135, 16865−16871

cysteine mutant *Tt*Ago (16 μM) storage buffer (500 mM NaCl, 20 mM Tris-HCl pH 7.5, 2 mM $MgCl_2$), and incubating it for 2 h at room temperature. To remove free dyes after labeling, we used Amicon Ultra-0.5 mL and 50K membrane (Millipore Corp. Billerica, MA) following the instruction provided by company.

Oligonucleotide Preparation. DNA guide oligonucleotides in which an amine modification was introduced with a six carbon linker at 18th base (g18, the exact modification is available in IDT Web site) were purchased from Integrated DNA technology (IDT, Coralville, IA and Figure S11). By using a conventional dye labeling protocol,[35] we labeled the guide strand with Cy5 monoNHS-ester (GE Healthcare), which reacts with the amine group on the guide strand. In case of the guide strand with the 3′-end amine modification at the 3′ OH of g21 (Figure 4 and Figure S11), a guide strand with Cy5 in the phosphate backbone between g18 and g19 was purchased from IDT. RNA target oligonucleotides were purchased from STpharm (South Korea), and conjugated with Cy3 at the 5′ phosphate. Labeled oligonucleotides were stored in T50 buffer containing 10 mM Tris-HCl (pH 8.0) with 50 mM NaCl. All nucleotide sequences are shown below, where mismatch bases were indicated by bold italic letters. Cy5-5′-phosphate-guide single strand DNA, 5′-p-TGA GGT AGT AGG TTG TAT(Cy5) AGT-3′; Cy3-target single strand RNA with no mismatch, 5′-(Cy3)ACU AUA CAA CCU ACU ACC UCG (poly 16U)-3′-biotin; Cy3-target single strand RNA with 10−11 mismatches, 5′-(Cy3)ACU AUA CAA C***UC*** ACU ACC UCG (poly 16U)-3′-biotin; Cy3-target single strand RNA with 20−21 mismatch, 5′-(Cy3)***UG***U AUA CAA CCU ACU ACC UCG (poly 16U)- 3′-biotin; Cy5-5′-phosphate-guide single strand RNA, 5′-p-UGA GGU AGU AGG UUG UAU(Cy5) AGU-3′.

Single-Molecule FRET Experiment. Single-molecule FRET experiments were performed in a total internal reflection fluorescence microscope. To reduce nonspecific binding of molecules, glass surface was coated with a mixture of PEG and biotin-PEG with 40:1 ratio.[35] A detection chamber was made between a quartz slide and a glass coverslip by using double-side sticky tape. To assemble Ago−guide complexes, 1 μM *Tt*Ago and 0.2 μM Cy5-labeled guide DNA or guide RNA was incubated for 30 min at 55 °C in a Ago−guide assembly buffer: 10 mM Tris-HCl (pH 8.0) with 100 mM NaCl and 5 mM $MgCl_2$. For single-molecule FRET experiments, target strand was immobilized on a quartz slide via streptavidin−biotin interaction, and diluted (usually by 100−500 times) preassembled Ago−guide complex in an imaging buffer (10 mM Tris-HCl (pH 8.0) with 135 mM KCl, a designated concentration of Mg^{2+}, and oxygen scavenger system: 4 mg/ml D-(+)-glucose (Sigma-Aldrich), 1 mg/ml glucose oxidase (Sigma-Aldrich), 0.04 mg/ml catalase (Roche), and saturating Trolox (25 mg/50 mL)) was injected into a detection chamber. Cy3 and Cy5 were excited by a 532-nm laser (Compass215M, Coherent, Santa Clara, CA) and a 640-nm laser (Cube640-100C, Coherent, Santa Clara, CA), respectively. To switch two lasers for alternative laser excitation (ALEX) experiment for Figures 3 and 4, mechanical shutters (LS-3, Uniblitz, Rochester, NY) were used. Fluorescence signals of Cy3, Cy5, and Alexa750 were collected through a water-immersion objective (UPlanSApo 60×, Olympus), separated by using two dichroic mirrors (635dcxr and 740dcxr, Chroma) and a mirror (BB01-E02, Thorlabs), and imaged on an EM-CCD camera (Ixon DV897, Andor). Scattered laser light was filtered out by using a long-pass filter for 535-nm (LP03-532RU-25, Semrock) and a notch filter for 640-nm (NF03-633E-25, Semrock, Rochester, NY). To control sample temperature, we used a specially designed temperature controller (Live Cell Instrument, South Korea) that maintains objective lens, prism, slide glass, and injecting solution at the same temperature. To solve the drifting and defocusing problems during long-time observation, home-built autofocusing and drift-correcting techniques were used.[43] Data were collected by using a home-built program written in Visual C++ (Microsoft), and analyzed by using Matlab 7.1 (MathWorks, Natick, MA) and Microcal Origin 8.5 (Microcal Software, Inc.). The analysis of hidden Markov modeling (HMM) was coded in Matlab based on the previous database.[44] To estimate the FRET states during FRET transitions, we performed HMM with two or three states. Background, bleed-through between channels, and gamma factors were corrected before data analysis.

■ ASSOCIATED CONTENT

Ⓢ Supporting Information

Supplemental figures referred to in the text. This material is available free of charge via the Internet at http://pubs.acs.org.

■ AUTHOR INFORMATION

Corresponding Authors

songj@kaist.ac.kr
shohng@snu.ac.kr

Author Contributions

⊥S.-R.J. and E.K. contributed equally to this work.

Notes

The authors declare no competing financial interest.

■ ACKNOWLEDGMENTS

This work was supported by Creative Research Initiatives (Physical Genetics Laboratory, 2009-0081562) and by WCU program of National Research Foundation of Korea (R31-10032) to S.H., and by the grants (NRF-2013R1A1A2A10005305, 2011-0020334, 2011-0031955) to J.-J.S. S.-R.J. thanks Sanghwa Lee, Hee-Soo Uhm and Jinwoo Lee for their helps in Matlab coding and three color FRET experiment. We also thank Yejin Lee for her technical assistance, and Dr. Chirlmin Joo and his lab members for critical reading of the manuscript.

■ REFERENCES

(1) Lee, R. C.; Feinbaum, R. L.; Ambros, V. *Cell* **1993**, *75* (5), 843−854.
(2) Wightman, B.; Ha, I.; Ruvkun, G. *Cell* **1993**, *75* (5), 855−862.
(3) Vagin, V. V.; Sigova, A.; Li, C.; Seitz, H.; Gvozdev, V.; Zamore, P. D. *Science* **2006**, *313* (5785), 320−324.
(4) Watanabe, T.; Totoki, Y.; Toyoda, A.; Kaneda, M.; Kuramochi-Miyagawa, S.; Obata, Y.; Chiba, H.; Kohara, Y.; Kono, T.; Nakano, T.; Surani, M. A.; Sakaki, Y.; Sasaki, H. *Nature* **2008**, *453* (7194), 539−543.
(5) Tam, O. H.; Aravin, A. A.; Stein, P.; Girard, A.; Murchison, E. P.; Cheloufi, S.; Anger, M.; Sachidanandam, R.; Schultz, R. M.; Hannon, G. J. *Nature* **2008**, *453* (7194), 534−538.
(6) Kim, V. N.; Han, J.; Siomi, M. C. *Nat. Rev. Mol. Cell. Biol.* **2009**, *10* (2), 1126−1139.
(7) Carthew, R. W.; Sontheimer, E. J. *Cell* **2009**, *136* (4), 642−655.
(8) Kawamata, T.; Tomari, Y. *Trends Biochem. Sci.* **2010**, *35* (7), 368−376.
(9) Kawamata, T.; Seitz, H.; Tomari, Y. *Nat. Struct. Mol. Biol.* **2009**, *16* (9), 953−960.
(10) Yoda, M.; Kawamata, T.; Paroo, Z.; Ye, X.; Iwasaki, S.; Liu, Q.; Tomari, Y. *Nat. Struct. Mol. Biol.* **2010**, *17* (1), 17−23.
(11) Lewis, B. P.; Shih, I. H.; Jones-Rhoades, M. W.; Bartel, D. P.; Burge, C. B. *Cell* **2003**, *115* (7), 787−798.
(12) Lewis, B. P.; Burge, C. B.; Bartel, D. P. *Cell* **2005**, *120* (1), 15−20.
(13) Ameres, S. L.; Martinez, J.; Schroeder, R. *Cell* **2007**, *130* (1), 101−112.
(14) Baek, D.; Villen, J.; Shin, C.; Camargo, F. D.; Gygi, S. P.; Bartel, D. P. *Nature* **2008**, *455* (7209), 64−71.
(15) Bartel, D. P. *Cell* **2009**, *136* (2), 215−233.
(16) Filipowicz, W.; Bhattacharyya, S. N.; Sonenberg, N. *Nat. Rev. Genet.* **2008**, *9* (2), 102−114.
(17) Haley, B.; Zamore, P. *Nat. Struct. Mol. Biol.* **2004**, *11* (7), 599−606.

(18) Parker, J. S.; Roe, S. M.; Barford, D. *EMBO J.* **2004**, *23* (24), 4727−4737.
(19) Song, J. J.; Smith, S. K.; Hannon, G. J.; Joshua-Tor, L. *Science* **2004**, *305* (5689), 1434−1437.
(20) Ma, J.-B.; Yuan, Y. R.; Meister, G.; Pei, Y.; Tushl, T.; Patel, D. J. *Nature* **2005**, *434* (7033), 666−670.
(21) Wang, Y.; Sheng, G.; Juranek, S.; Tuschl, T.; Patel, D. J. *Nature* **2008a**, *456* (7219), 209−213.
(22) Wang, Y.; Juranek, S.; Li, H.; Sheng, G.; Tuschl, T.; Patel, D. J. *Nature* **2008b**, *456* (7224), 921−926.
(23) Liu, J.; Carmell, M. A.; Rivas, F. V.; Marsden, C. G.; Thomson, J. M.; Song, J. J.; Hammond, S. M.; Joshua-Tor, L.; Hannon, G. J. *Science* **2004**, *305* (5689), 1437−1441.
(24) Rivas, F. V.; Tolia, N. H.; Song, J.-J.; Aragon, J. P.; Liu, J.; Hannon, G. J.; Joshua-Tor, L. *Nat. Struct. Mol. Biol.* **2005**, *12* (4), 340−349.
(25) Lingel, A.; Simon, B.; Izaurralde, E.; Sattler, M. *Nature* **2003**, *426* (6965), 465−469.
(26) Song, J. J.; Liu, J.; Tolia, N. H.; Schneiderman, J.; Smith, S. K.; Martienssen, R. A.; Hannon, G. J.; Joshua-Tor, L. *Nat. Struct. Biol.* **2003**, *10* (12), 1026−1032.
(27) Yan, K. S.; Yan, S.; Faroog, A.; Han, A.; Zeng, L.; Zhou, M. M. *Nature* **2003**, *426* (6965), 468−474.
(28) Elbashir, S. M.; Lendeckel, W.; Tuschl, T. *Genes Dev.* **2001a**, *15* (2), 188−200.
(29) Elbashir, S. M.; Martinez, J.; Patkaniowska, A.; Lendeckel, W.; Tuschl, T. *EMBO J.* **2001b**, *20* (23), 6877−6888.
(30) Nykänen, A.; Haley, B.; Zamore, P. D. *Cell* **2001**, *107* (3), 309−321.
(31) Parker, J. S.; Parizotto, E. A.; Wang, M.; Roe, S. M.; Barford, D. *Mol. Cell* **2009**, *33* (2), 204−214.
(32) Filipowicz, W. *Cell* **2005**, *122* (1), 17−20.
(33) Tomari, Y.; Zamore, P. D. *Genes Dev.* **2005**, *19* (5), 517−529.
(34) Wang, Y.; Juranek, S.; Li, H.; Sheng, G.; Wardle, G. S.; Tuschl, T.; Patel, D. J. *Nature* **2009**, *461* (7265), 754−761.
(35) Roy, R.; Hohng, S.; Ha, T. *Nat. Methods* **2008**, *5* (6), 507−516.
(36) Elkayam, E.; Kuhn, C.-D.; Tocilj, A.; Haase, A. D.; Greene, E. M.; Hannon, G. J.; Joshua-Tor, L. *Cell* **2012**, *150* (1), 100−110.
(37) Nakanishi, K.; Weinberg, D. E.; Bartel, D. P.; Patel, D. J. *Nature* **2012**, *486* (7403), 368−374.
(38) Schirle, N. T.; MacRae, I. J. *Science* **2012**, *336* (6084), 1037−1040.
(39) Wee, L. M.; Flores-Jasso, C. F.; Salomon, W. E.; Zamore, P. D. *Cell* **2012**, *151* (5), 1055−1067.
(40) Lee, S.; Lee, J.; Hohng, S. *PLoS One* **2010**, *5* (8), e12270.
(41) Schwarz, D. S.; Hutvagner, G.; Haley, B.; Zamore, P. D. *Mol. Cell* **2002**, *10* (3), 537−548.
(42) Gu, S.; Jin, L.; Huang, Y.; Zhang, R.; Kay, M. A. *Curr. Biol.* **2012**, *22* (16), 1536−1542.
(43) Hwang, W.; Bae, S.; Hohng, S. *Opt. Express* **2012**, *20* (28), 29353−29360.
(44) Bronson, J. E.; Fei, J.; Hofman, J. M.; Gonzalez, R. L., Jr.; Wiggins, C. H. *Biophys. J.* **2009**, *97* (12), 3196−3205.